의학박사 학위논문

In vivo study to optimize treatment schedule for the lung stereotactic ablative radiotherapy based on the real-time changes in tumor hypoxia

실시간 종양 내 저산소화 변화에 기반
체부정위방사선치료 스케줄 최적화를 위한
in vivo 연구

2016 년 8 월

서울대학교 대학원
의학과 방사선종양학 전공
송 창 훈

의학박사 학위논문

In vivo study to optimize treatment schedule for the lung stereotactic ablative radiotherapy based on the real-time changes in tumor hypoxia

실시간 종양 내 저산소화 변화에 기반
체부정위방사선치료 스케줄 최적화를 위한
in vivo 연구

2016 년 8 월

서울대학교 대학원
의학과 방사선종양학 전공
송 창 훈

In vivo study to optimize treatment schedule for the lung stereotactic ablative radiotherapy based on the real-time changes in tumor hypoxia

지도교수 김 학 재

이 논문을 의학박사 학위논문으로 제출함

2016 년 4 월

서울대학교 대학원

의학과 방사선종양학 전공

송 창 훈

송창훈의 의학박사 학위논문을 인준함

2016 년 7 월

위 원 장 _____ (인)

부 위 원 장 _____ (인)

위 원 _____ (인)

위 원 _____ (인)

위 원 _____ (인)

Abstract

In vivo study to optimize treatment schedule for the lung stereotactic ablative radiotherapy based on the real-time changes in tumor hypoxia

Changhoon Song

Medical Science (Radiation Oncology)

The Graduate School

Seoul National University

Introduction: An optimal interval between the fractionation sessions of stereotactic ablative radiotherapy (SABR) has not been established. Understanding of temporal changes in tumor hypoxia can provide clues for the optimal fractionation intervals and potentially lead to improved therapeutic outcomes by SABR. In this study, we hypothesized that serial *in vivo* measurements of tumor hypoxia after a single high-dose irradiation in a mouse model of subcutaneous and orthotopic lung cancer would be done by [^{18}F]-misonidazole (F-MISO) positron emission tomography (PET) and hypoxia-responsive element (HRE)-driven bioluminescence imaging and we also hypothesized that tumor hypoxia would return to pretreatment levels at 6 hours ~ 6 days after irradiation in murine lung carcinoma model.

Methods: Syngeneic Lewis lung carcinomas were grown either subcutaneously in the back or orthotopically in the lung of C57BL/6 mice and

irradiated with a single dose of 15 Gy to mimic SABR used in the clinic. Serial F-MISO PET imaging was performed before irradiation (day –1), at 6 hours (day 0), and 2 (day 2) and 6 (day 6) days after irradiation for both subcutaneous and orthotopic lung tumors. For F-MISO, the tumor-to-background activity ratio (TBR) was analyzed. Serial HRE-driven bioluminescence imaging was performed at 6 hours, 1 day, 2 and 6 days after irradiation. Pimonidazole fluorescent activated cell sorting (FACS) analysis and Hoechst 33342 vascular perfusion combined with immunostaining, were also performed to further explain the findings of F-MISO PET and bioluminescence imaging.

Results: In subcutaneous tumors, the maximum TBR was 2.87 ± 0.483 at day –1, 1.67 ± 0.116 at day 0, 2.92 ± 0.334 at day 2, and 2.13 ± 0.385 at day 6, indicating that tumor hypoxia was decreased immediately after irradiation and had returned to the pretreatment levels at day 2 after radiation. Hypoxic signals were too low to quantitate for orthotopic tumors using F-MISO PET or HRE-driven bioluminescence imaging. Pimonidazole FACS analysis also revealed similar patterns, in which pimonidazole-positive cell populations were decreased immediately after irradiation followed by a recovery to the pretreatment levels. Using Hoechst 33342 vascular perfusion dye, CD31 and cleaved caspase 3 co-immunostaining, we found a rapid and transient vascular collapse, which might have resulted in poor intratumor perfusion of F-MISO PET tracer or pimonidazole delivered at day 0, leading to decreased hypoxic signals at day 0 by PET or pimonidazole analyses.

Conclusions: F-MISO PET and HRE-driven bioluminescence imaging can measure temporal changes of individual tumor hypoxia not in the orthotopic lung tumor model but in the subcutaneous lung tumor model. After a single high-dose of irradiation in murine subcutaneous lung carcinoma model, the level of tumor hypoxia returned to the pretreatment level by 2 days. Our

results also indicate that a single high-dose irradiation can produce a rapid, but reversible, vascular collapse in tumors.

* This work is published in the International Journal of Radiation Oncology Biology Physics (International journal of radiation oncology, biology, physics. 2016;95(3):1022-31).

Keywords: Lung cancer, hypoxia, positron-emission tomography, radiotherapy, dose fractionation

Student Number: 2013-30548

Contents

List of Figures

Introduction

Lung cancer is the leading cause of cancer death in the world (1) and also in Korea (2). The incidence of early stage non-small cell lung cancer (NSCLC) among the elderly is expected to rise dramatically due to screening with low-dose computed tomography (CT) scan (3). Surgical resection for early stage NSCLC remains the only reliable treatment for cure. However, almost one third of patients with early stage NSCLC do not have surgery due to old age, multiple comorbidities, or patients′ refusal for surgery (4).

Stereotactic ablative radiotherapy (SABR; also known as stereotactic body radiotherapy (SBRT)), defined as the precise delivery of high doses of radiation within a few fractions (5), has become standard of care for patients with stage I NSCLC whom are unable to tolerate surgery (6, 7), and has even been considered a valid alternative to surgery in those of operable patients (8, 9). SABR has produced superb local control rates exceeding 90% in many prospective clinical trials (10-15). However, many patients enrolled in those trials might not have fully reflected the full spectrum of patients encountered in everyday clinical practice, and we still need to devise strategies to improve the local control by SABR.

It is well known that tumor hypoxia is a poor prognostic factor for radiotherapy contributing to the resistance to therapies (16, 17) and increasing a metastatic potential (18). A number of studies have shown that tumor hypoxia also exists and is a poor prognostic factor in NSCLC (19-23), indicating that overcoming tumor hypoxia might significantly benefit patients with NSCLC treated by SABR. Compared with the single treatment session, fractionated irradiation effectively kills hypoxic tumor cells utilizing a phenomenon of reoxygenation, the process by which hypoxic cells surviving

at the given radiation dose become oxygenated before the next radiation dose (24, 25). Although SABR is currently preferred to be given in 4 to 5 fractions than 1 to 3 fractions (26), an optimal interval between the fractionation sessions has not been established. Various fractionation schedules are being used intuitively, including 48 Gy in 4 fractions within 4 to 8 days, 50 Gy in 5 fractions within 5 to 13 days, or 45 to 60 Gy in 3 fractions within 5 to 14 days (10, 12, 15, 27, 28). Considering that the presence of a tumor hypoxic fraction of even 10% can potentially decrease the amount of cell kill produced by high-dose hypofractionated irradiation by nearly 3 orders of magnitudes (29), it would seem most logical to set an optimal treatment schedule for SABR according to the temporal changes in tumor hypoxia between the fractionation intervals.

Previously several *ex vivo* studies have investigated hypoxia changes after high-dose irradiation in various subcutaneous murine tumor models (30-33) including lung cancer model (30). Kim *et al*. observed that immediately after single irradiation of 10 Gy, tumor hypoxia increased and rapidly returned to pretreatment levels at 3 ~ 6 hours after irradiation in murine squamous cell carcinoma (31). Another study has shown that reoxygenation after single irradiation of 13 to 15 Gy is not complete at 24 hours after irradiation and proceeds further until 72 hours or thereafter in murine squamous cell carcinoma, mammary carcinoma, and fibrosarcoma (32). Lan *et al*. demonstrated by using immunostaining that reoxygenation was not observed at 3 days after ablative irradiation, but was observed at 8, 15, 21 days after ablative irradiation in Lewis lung carcinomas (30). Interestingly, Chen *et al.* insisted via immunostaining that ablative irradiation causes chronic and persistent hypoxia in murine prostate cancer (33). These differences may be attributed to the use of different types of tumors and the heterogeneity of tumor hypoxia at the inter- and intra-individual levels.

Therefore it would be the most logical to understand the temporal changes in tumor hypoxia between the fractionation intervals and this could ideally be done by performing serial *in vivo* measurements of tumor hypoxia in the same subject. In this regard, [^{18}F]-misonidazole (F-MISO) positron emission tomography (PET) imaging is highly attractive, because it allows serial clinically relevant noninvasive, *in vivo* quantification of tumor hypoxia on the same subject and has been validated against the reference standard polarographic oxygen-sensitive electrodes for tumor hypoxia measurements in both preclinical and clinical settings (34-36).

While PET imaging is clinically relevant, there are some limitations including radioactive isotope and tracer availability, technical difficulties of multiple injections of PET tracers, and the need for sufficiently large tumors for detection. Bioluminescence imaging is also being widely used experimentally due to its sensitivity and efficiency. To image tumor hypoxia by bioluminescence, we utilized hypoxia-responsive element (HRE)-driven bioluminescence system, in which hypoxia-inducible factor (HIF) only being stabilized under hypoxic conditions binds to HRE thereby driving luciferase expression (37-39).

On the while, subcutaneous tumor model cannot represent the real tumor in real environment. More sophisticated orthotopic tumor model in which tumor cells are implanted and grown within the organ from which they were derived allows organotypical interaction between tumor cells and surrounding stroma. Thus, orthotopic tumor model can mimic natural environment of tumorigenesis (40). Recently, Liu *et al.* have reported that the tumor-forming rate of the orthotopic lung cancer cell line A549 was 90% in BALB/c nude mice via direct intrathoracic injection (41).

In this study, we hypothesized that serial *in vivo* measurements of tumor hypoxia after a single high-dose irradiation in a mouse model of

subcutaneous and orthotopic lung cancer would be done by F-MISO PET and HRE-driven bioluminescence imaging and we also hypothesized that tumor hypoxia would return to pretreatment levels at 6 hours ~ 6 days after irradiation in murine lung carcinoma model.

Other preclinical analyses, including pimonidazole fluorescent activated cell sorting (FACS) analysis and Hoechst 33342 vascular perfusion combined with immunostaining, were also performed to further explain the findings of F-MISO PET and bioluminescence imaging.

Materials and Methods

Animal model and tumor implantation

All animal experiments were conducted under the guidelines approved by the institutional animal care and use committee of the Seoul National University Hospital (approval no. 14-0137-S1A2), and Pohang University of Science and Technology (approval no. POSTECH-2015-0039). Lewis lung carcinoma cells expressing luciferase were purchased from Caliper (Caliper Life Sciences, Hopkinton, MA, USA) and were cultured in Roswell Park Memorial Institute 1640 (ATCC, Manassas, VA, USA) medium supplemented with 10% fetal bovine serum (Lonza BioWhittaker, Walkersville, MD, USA). Cancer cells were grown subcutaneously or orthotopically in 6-week-old male C57BL/6 mice (Orient Bio Inc., Seongnam, Korea). To produce tumors mice were firstly anesthetized with intraperitoneal injection of ketamine (80 mg/kg)/xylazine (16 mg/kg) cocktail made in saline. For subcutaneous tumors, 5 x 10^5 tumor cells were injected beneath the skin on the lower back of a mouse. To implant tumor cells in the orthotopic lung location, an incision was made on the left lateral side of the thorax, followed by injection of tumor cell suspension (5 x 10^5 tumor cells/50 μl) into the upper margin of the sixth rib on the left anterior axillary line to the depth of 5mm. The incision was then sutured. Tumor formation was monitored and confirmed by bioluminescence imaging (IVIS 100 imaging system, Perkin Elmer, Waltham, MA, USA) via intraperitoneal injection of luciferin (Caliper Life Sciences).

To further validate the results with PET imaging, another independent assay in which tumor hypoxia was monitored by HRE-driven bioluminescence was performed. Lewis lung carcinoma expressing either

constitutive luciferase or transfected with 5X HRE-luciferase plasmid (a generous gift from Professor J. Martin Brown, Stanford University, Stanford, CA, USA) were used. Serial HRE-bioluminescence imaging was performed at 6 hours (day 0), 1 day (day 1), 2 (day 2), and 6 (day 6) days after irradiation for similarly established subcutaneous and orthotopic lung tumors.

Irradiation and micro-PET imaging

At 13 days after subcutaneous and 8 days after orthotopic tumor implantation, the mice were anesthetized as reported and irradiated with 6-MV x-ray from a linear accelerator (Varian Medical System, Palo alto, CA, USA) at the Seoul National University Hospital or by Precision X-ray 320 small animal irradiator (North Branford, CT, USA) at Pohang University of Science and Technology, at a single dose of 15 Gy to mimic SABR used in the clinic (Figure 1).

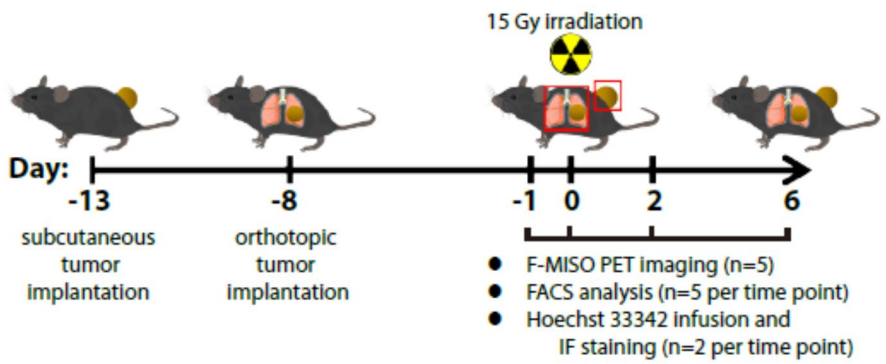

Figure 1. A scheme outlining experimental design.

Serial F-MISO PET imaging 1 day before irradiation (day –1) and at 6 hours (day 0), 2 days (day 2), and 6 days (day 6) after irradiation was performed for both subcutaneous and orthotopic models. F-MISO (1.85 MBq/0.1 ml) was intravenously injected and image was obtained at 2 hours after tracer

administration for 3 minutes (static images). We chose a 2-hour waiting time given the trade-off between F-MISO uptake in target tissues and signal-to-noise ratios, although longer waiting times could yield higher F-MISO washout in the background tissues. The mice were anesthetized with a 2% isoflurane-to-air mixture during PET scanning (GENISYS^4 small-animal PET scanner, Sofie Biosciences, Culver City, CA, USA). Acquired 3-dimensional emission data were reconstructed by an iterative reconstruction algorithm (ordered-subset expectation maximization) without attenuation correction. Image visualization and volume of interest (VOI) delineation were performed using AMIDE software (Stanford University, CA, USA). VOIs of orthotopic lung tumors and subcutaneous tumors were drawn manually on PET images, and maximal activity of each VOI was measured. The brain was chosen as the reference tissue because it has previously been shown to have a similar low uptake for F-MISO compared with other tissues, such as the muscle, which are normally used as reference tissues in other studies (42, 43). Spherical VOIs (3-mm radius) were drawn in the brain to measure the mean activity, and tumor-to-background ratio (TBR) of radioactivity was calculated as the maximal activity in the tumor region divided by the mean activity in the background region. To delineate the VOIs accurately, CT images taken 3 days after irradiation were used as anatomical reference images.

Pimonidazole FACS analysis

The mice were injected with pimonidazole (60 mg/kg; Hypoxyprobe Inc., Burlington, MA, USA) 1 hour prior to sacrifice. Subcutaneously implanted tumor was harvested and went through mechanical digestion and enzyme digestion. Enzyme digestion was performed using enzyme cocktail

including Collagenase Type I (Worthington, NJ, USA), Pronase (EMD Millipore, Billerica, MA, USA), DNase (Sigma-Aldrich, St. Louis, MO, USA) in 1X HBSS (Life technologies, Waltham, Boston, MA, USA) for 40 minutes. Digested subcutaneously implanted tumor was then filtered with cell strainer (BD Biosciences, Franklin Lakes, NJ, USA) and spin down (5 minutes, 1600 rpm, 4°C). Lung was harvested and grinded on the cell strainer (BD Biosciences) using syringe plug (BD Biosciences) with PBS (phosphate-buffered saline; Bioneer, Daejeon, Korea) and the cells were spin down (5 minutes, 1600 rpm, 4°C). Subcutaneously implanted tumors and lung tumors were both resuspended with 1X Pharm Lyse RBC lysis buffer (BD Biosciences), filtered with filter tip tube (BD Biosciences) and incubated for 10 minutes in ice and spin down (5 minutes, 1600 rpm, 4°C). Each samples were resuspended with 0.5 ml of FACS buffer and filtered with filter tip tube (BD Biosciences). Cells were treated with 0.5 μl of Pimonidazole primary antibody (Hypoxyprobe Inc.) and incubated for 25 minutes in ice and were spin down (5 minutes, 1600 rpm, 4°C) for washing step. Cells were then treated with 0.5 μl of anti-rabbit 647 secondary antibody (Invitrogen, Carlsbad, CA, USA) and incubated for 25 minutes in ice. After incubation, cells were spin down for 5 minutes in 1600rpm 4°C and resuspended with 1ml FACS buffer, filtered with filter tip tube (BD Biosciences) and analyzed using LSR Fortessa cell analyzer (BD Biosciences).

Immunohistochemistry

Lung tissues were embedded in optimum cutting temperature (OCT) compound (Sakura Finetek, Torrance, CA), and frozen in -80°C until cryosectioning. The lung tissue sections were post-fixed with 4% paraformaldehyde for 20 minutes at irradiation prior to the staining. For

quenching the tissue peroxidase, the sections were incubated with 5% H_2O_2 for 30 minutes at irradiation. To avoid non-specific binding, blocking was performed with 1% bovine serum albumin in 0.3% Triton X-100 for 1 hour and 15 minutes. Immunohistochemistry was performed with monoclonal mouse antibodies for pimonidazole (1:1000; Hypoxyprobe Inc.) for 4 hours at irradiation. Secondary antibodies were goat anti-rabbit IgG-horse radish peroxidase (Santa Cruz Biotechnology, Santa Cruz, CA, USA) and incubated for 1.5 hours at room temperature. The sections were further incubated with streptavidin-horse radish peroxidase (BD Biosciences) for 1 hour and developed with Peroxidase Substrate Kit (Vector Laboratories, Inc., Burlingame, CA, USA) for 10 minutes at irradiation, counterstained with methyl green (Vector Laboratories, Inc.) and after drying were mounted with Vecta Mount (Vector Laboratories, Inc.). The sections were finally examined with a Leica DM750 microscope with a 4x objective lens. Mice which had received no pimonidazole served as a biological negative control for pimonidazole staining. None of the negative controls showed any reactivity.

Hoechst 33342 perfusion and immunostaining

Hoechst 33342 (Sigma-Aldrich) was dissolved in sterile water at 4 mg/ml concentrations and 200 μg was injected intravenously to mice. Mice were sacrificed within 1 minute after injection by cervical dislocation and the tumors were excised and mounted with OCT medium (Sakura Finetek).

Tumors were embedded in OCT compound, and frozen in -80°C until cryosectioning and immunostaining. For CD31 immunostaining, the tumor sections were post-fixed with 100 % methanol for 10 minutes at irradiation prior to the staining. The sections were incubated with 0.5% Triton X-100 in

PBS for 5 minutes, followed by incubation with rat anti-mouse CD31 monoclonal antibodies (BD Biosciences) for overnight at 4°C. Secondary antibodies were anti-rat Alexa 546 (Life technologies) and incubated for 2 hours at room temperature. The sections were finally mounted with ProLong Gold antifade reagent (Life technologies), and examined with a Zeiss Axio Scope (EC Plan-Neofluar at 10x objective lenses). Digital images were taken using AxioCam HRM camera and processed with AxioVision 4.8 software. Quantification was performed by choosing ≥5 viable regions of tumors randomly and analyzed for the pixel intensity using Image J software (National Institute of Health, Bethesda, MD, USA).

Statistical analyses

Statistical comparisons of the data sets were performed using 1-way analysis of variance using Prism software, version 4.00 (GraphPad Inc., La Jolla, CA, USA) with the Tukey post-test and considered significant at $P < 0.05$.

Results

F-MISO PET imaging

For PET imaging, we intravenously administered 4 consecutive doses of F-MISO to 24 mice bearing well-established subcutaneous and orthotopic lung tumors, confirmed by bioluminescence imaging (Figure 2). Among these, 17 mice completed F-MISO injections and 9 mice (5 subcutaneous and 4 orthotopic tumor-bearing mice) were analyzed to yield TBR values.

Representative PET images demonstrating F-MISO uptake in subcutaneous tumor are shown in Figure 3A. In subcutaneous tumors, all 5 tumors demonstrated moderate F-MISO uptake, indicating that these tumors contained hypoxic regions before irradiation (Figure 3B). The mean and standard error of the mean of the maximum TBR values for these 5 tumors were 2.87 ± 0.483 at day –1, 1.67 ± 0.116 at day 0, 2.92 ± 0.334 at day 2, and 2.13 ± 0.385 at day 6 after irradiation (Figure 3C), demonstrating an immediate and significant (P = 0.0497) decrease in TBR after irradiation, followed by a return to the pretreatment level at day 2 and a further decrease at day 6.

In orthotopic tumors, although we were able to locate tumors using microcomputed tomography scan (Figure 4), an elevated uptake of F-MISO greater than background was not evident, except for only a few mice (representative high and low F-MISO uptake in orthotopic tumors is shown in Figure 4A and 4B, respectively). This made it difficult to conduct TBR analyses of F-MISO PET in these orthotopic tumors. It is likely that these orthotopic tumors were too small to yield significantly detectable hypoxic PET imaging in the present study.

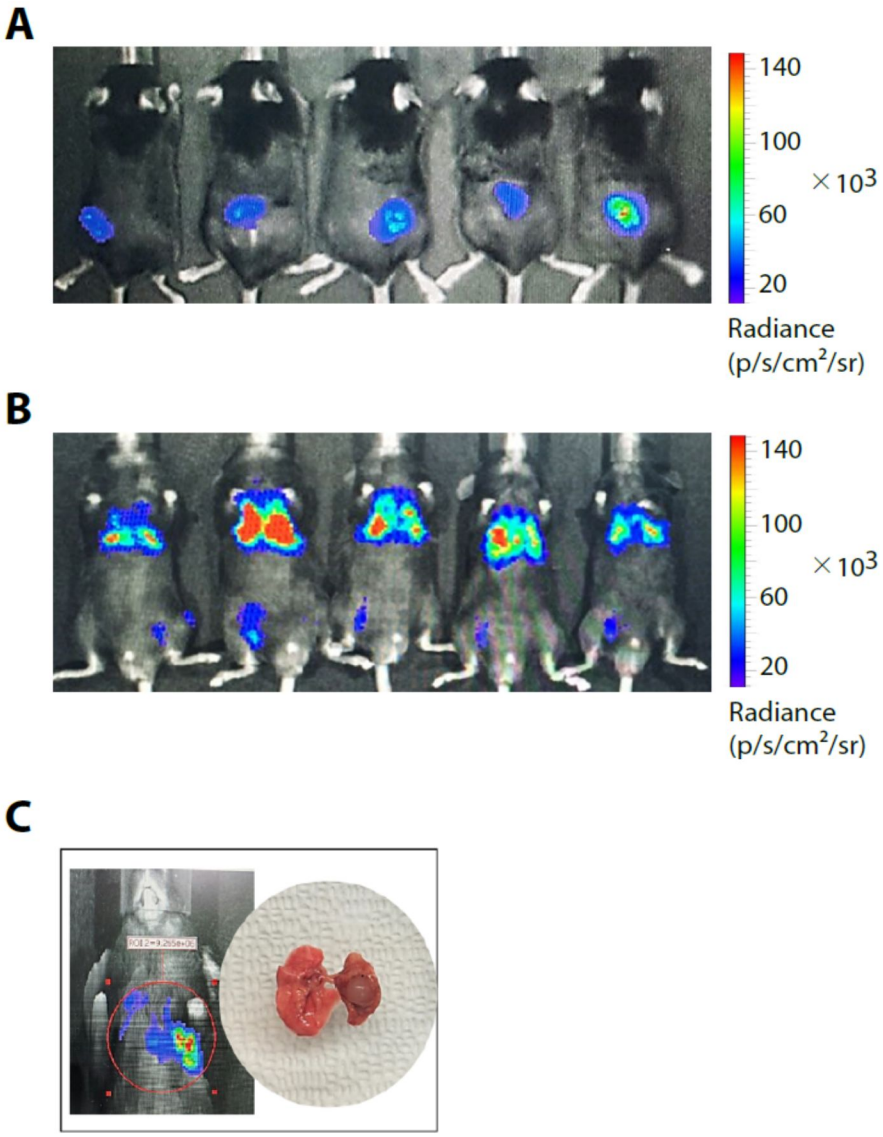

Figure 2. *In vivo* bioluminescence images for subcutaneous (A) and orthotopic (B) tumor-bearing mice. (C) A photograph showing macroscopic orthotopic lung tumors.

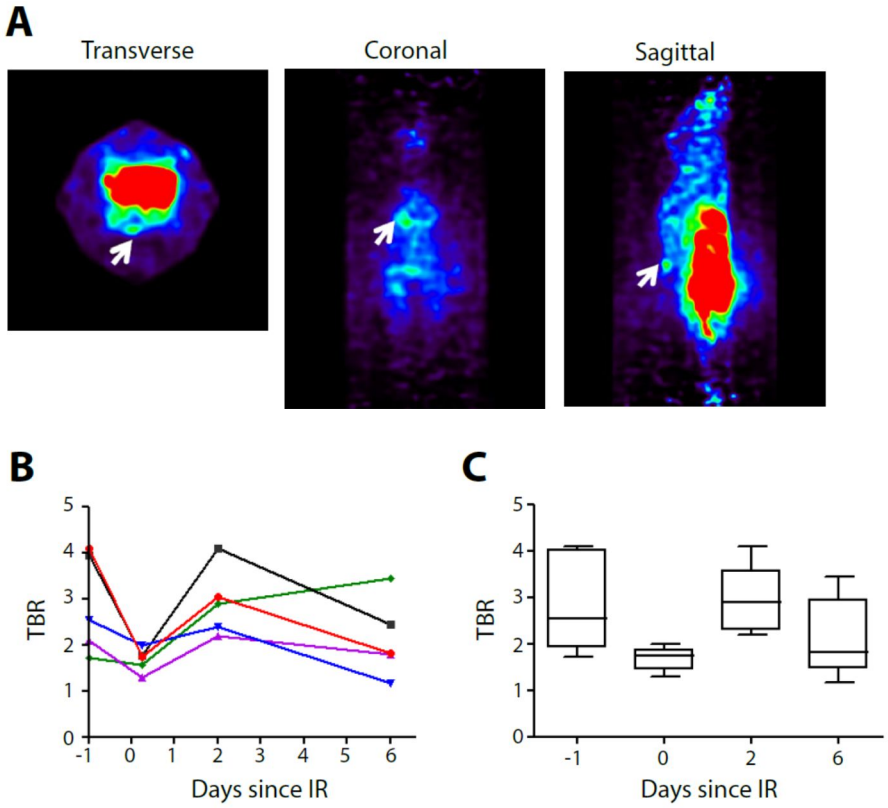

Figure 3. Temporal changes in tumor hypoxia for subcutaneous tumors by F-MISO PET imaging. (A) Representative PET images demonstrating F-MISO uptake in subcutaneous tumor. Arrows indicate the tumor position. (B) A graph showing the change in maximum TBR values for each individual animal. (C) A graph showing the mean ± s.e.m. of the maximum TBR values in Panel B (n = 5).

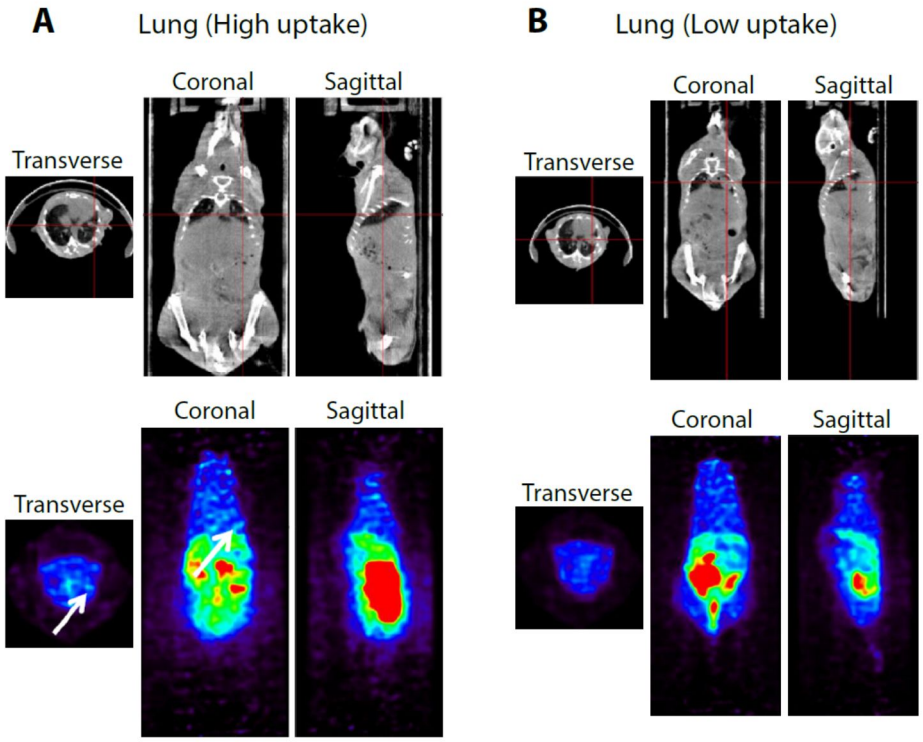

Figure 4. F-MISO uptake in orthotopic lung tumors. Computed tomography (top panels) and F-MISO PET (bottom panels) images for orthotopic lung tumor-bearing mice demonstrating high (A) or low (B) uptake of F-MISO. Arrows indicate the tumor position.

HRE-luciferase bioluminescence imaging

To validate the results with PET imaging, we performed a similar independent experiment in which we orthotopically implanted cancer cells that had been transfected with HRE-driven luciferase. We consistently observed that HRE-driven hypoxic signals were too low to yield meaningful quantification for hypoxia-driven luciferase signals in orthotopic lung tumors (Figure 5). Using such cells in subcutaneous tumors, we were able to observe hypoxia-driven luciferase signals (Figure 6). However, the HRE-driven luciferase bioluminescence was not different between irradiated and unirradiated tumors and remained consistently low during the 6 days we examined it (Figure 6). Importantly, the irradiated subcutaneous tumor volume measured by bioluminescence did not change significantly over time, but the unirradiated tumor volume progressively increased (Figure 6), suggesting that the dynamics of tumor hypoxia we examined above (Figure 3) could not simply be predicted by a change in the tumor volume.

Pimonidazole FACS analysis

Our results in subcutaneous tumors demonstrating the sudden decrease in F-MISO signals immediately after irradiation (Figure 3B and 3C) led us to examine the extent of hypoxic tumor cells in more details. To do this, we first examined pimonidazole-positive tumor cell populations in mice bearing subcutaneous and orthotopic lung tumors, as described in Figure 1, in which pimonidazole was injected before tumor harvest and FACS analysis. Pimonidazole is a nitroimidazole compound similar to misonidazole used in F-MISO, which undergoes a hypoxic-selective chemical modification, yielding cellular adducts in hypoxic cells (44). Similar to our PET imaging results, we observed an immediate decrease in pimonidazole-positive cell

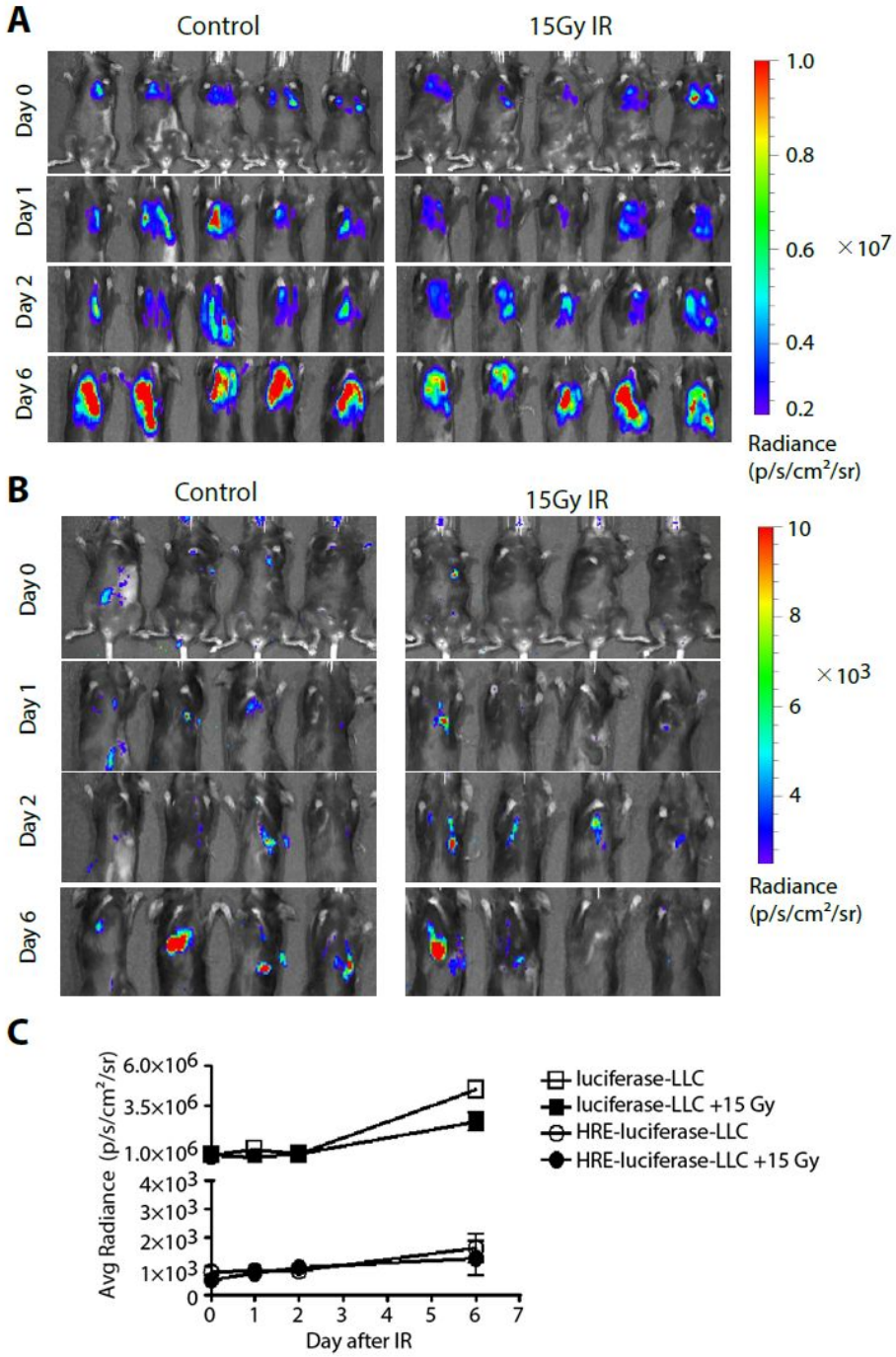

Figure 5. Bioluminescence imaging (BLI) of mice bearing orthotopic tumors with constitutive luciferase (A) or hypoxia-responsive element-driven luciferase (B) expression. Mice in A and B were either unirradiated (control)

or irradiated at 15 Gy (15 Gy IR) prior to imaging. (C) Photon BLI was quantified in each group. Symbols indicate the mean ± s.e.m. of photon counts of BLI for each group ($n \geq 4$ mice per group).

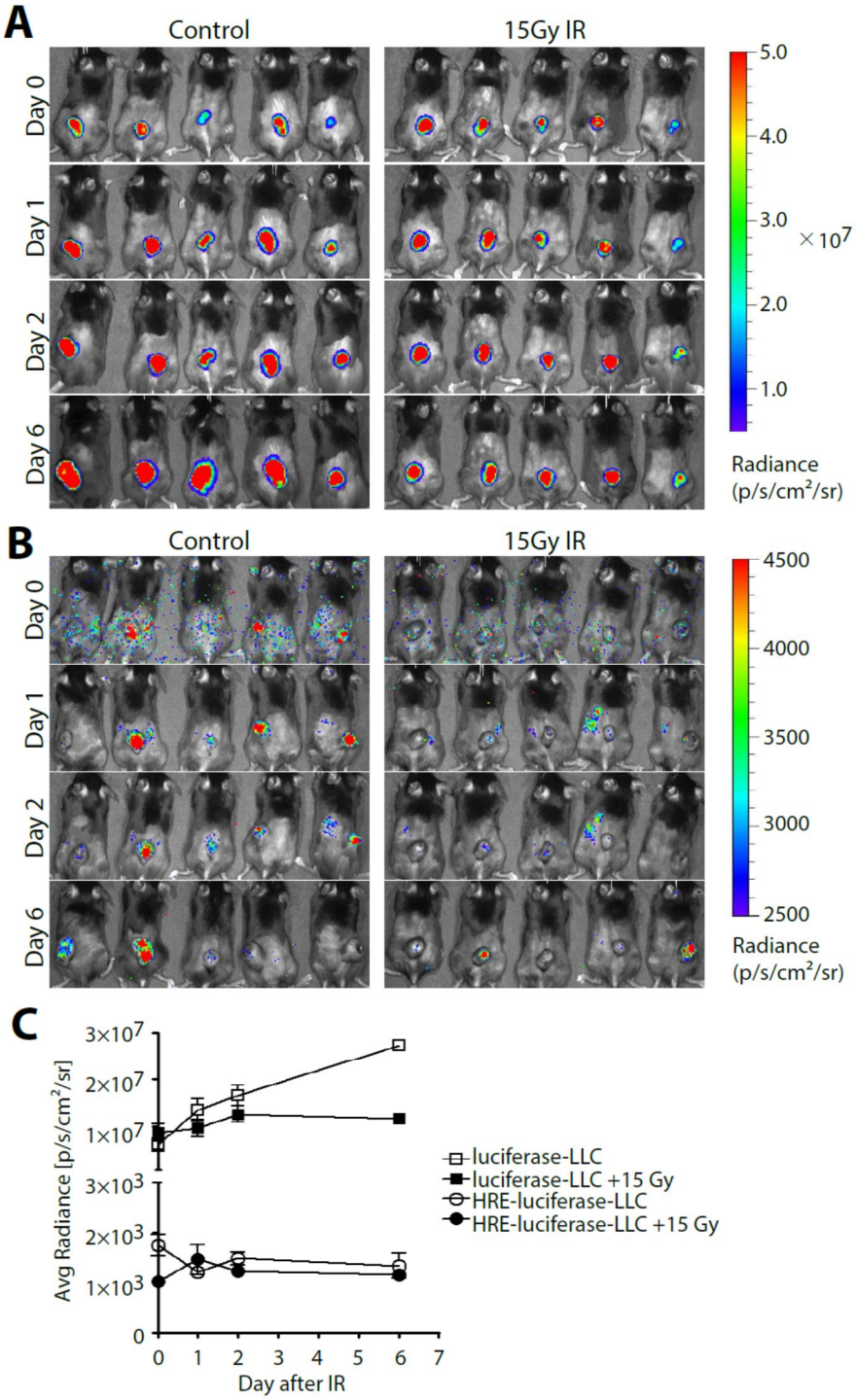

Figure 6. Bioluminescence imaging (BLI) of subcutaneous tumors expressing constitutive luciferase (A) or hypoxia-responsive element-driven

luciferase (B) expression, either unirradiated (control) or irradiated at 15 Gy (15 Gy IR). (C) Photon BLI was quantified in each group. Symbols indicate the mean ± s.e.m. of photon counts of BLI for each group (n = 5 mice per group).

populations after irradiation, which had then returned to (Figure 7A and 7B) or had even increased in subcutaneous tumors (Figure 7A) to the preirradiated levels by days 2 and 6 after irradiation. In orthotopic tumors, we noticed an unusually high level of pimonidazole-positive cell populations (Figure 7B), likely owing to the tissue-intrinsic artifacts in the lung, because we also observed high pimonidazole-positive cells, even in the normal lung free of tumors (Figure 7C and 8).

Hoechst 33342 perfusion and immunostaining

Our results demonstrating an immediate decrease in hypoxic signals in subcutaneous tumors by F-MISO or pimonidazole suggest it is possible that tumors became better oxygenated immediately after irradiation. However, it does not exclude the possibility of vascular damage that can be produced by the high-dose irradiation (19, 45, 46), which might have subsequently caused an insufficient perfusion of hypoxic tracers (F-MISO and pimonidazole) into the tumors. To test this possibility, we intravenously injected a vascular perfusion dye, Hoechst 33342, into mice bearing subcutaneous and orthotopic lung tumors immediately prior to sacrifice. We found that intratumor perfusion of Hoechst 33342 was markedly reduced, and blood vessel morphology was altered at 6 hours (i.e., day 0) after radiation for both subcutaneous (Figure 9A-9C) and orthotopic (Figure 9E-9G) tumors. To examine whether the decreased Hoechst 33342 would have resulted from vascular damage, we also stained subcutaneous tumors for cleaved caspase-3 (CC3), a well-known executer molecule for cellular apoptosis (47). We found that approximately 50 % of the blood vessels were positive for CC3 at day 0 (Figure 9D), indicating massive endothelial cell apoptosis, which might mediate the reduced intratumor perfusion of Hoechst 33342. At days 2 and 6,

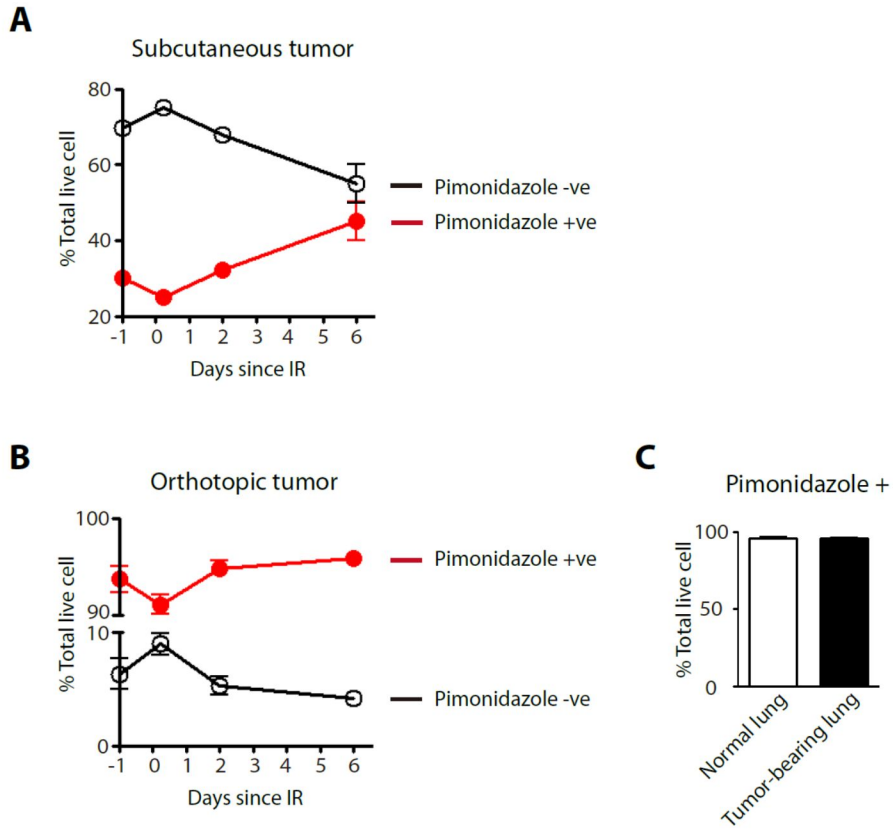

Figure. 7. Temporal changes in tumor hypoxia by pimonidazole FACS analyses. Pimonidazole-positive (red) and pimonidazole-negative (black) populations are shown for subcutaneous (A) and orthotopic (B) lung tumors in mice (symbols indicate mean ± s.e.m. for 5 mice per group per time point). (C) Pimonidazole-positive populations in the normal lung tissues (not bearing tumors) or lung tissues bearing tumors at day 6. Note that high background for pimonidazole in the lung tissues. Symbols presented as the mean ± s.e.m. for 5 mice per group. Abbreviations: −ve = negative; +ve = positive; IR = ionizing radiation.

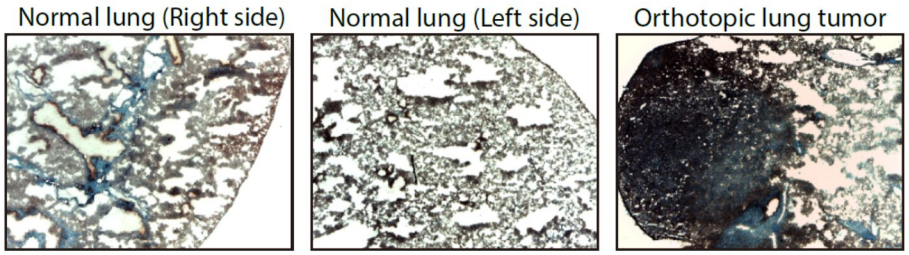

Figure 8. Pimonidazole immunostaining of the normal lung (free of tumors) or orthotopic lung tumors. Note that there is a background false-positive signals in the normal lung tissues.

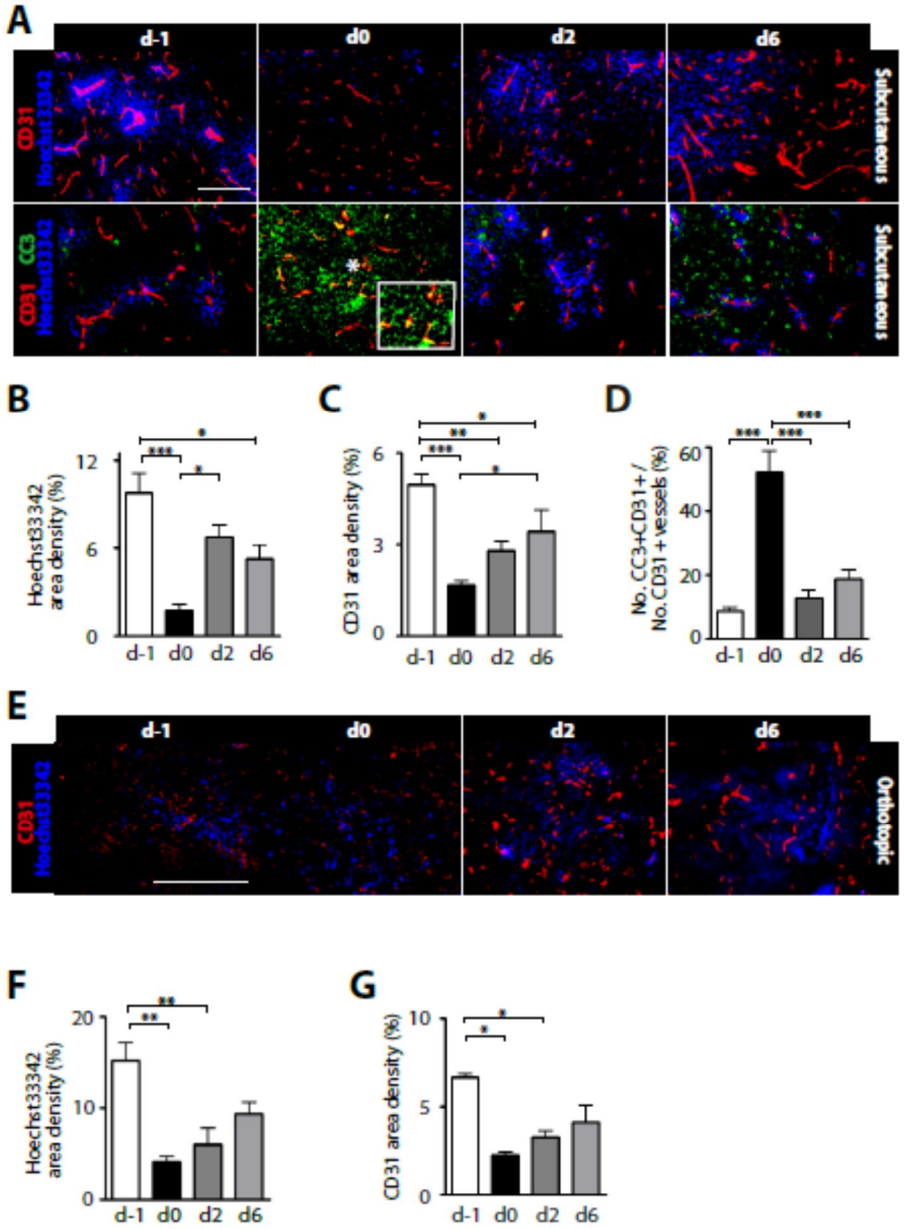

Figure 9. High ablative dose of irradiation causes a rapid and transient vascular collapse in tumors. (A) Subcutaneous tumors showing Hoechst 33342 perfusion dye (blue), CD31 (red) or CC3 (cleaved caspase-3; green) co-immunostaining. Insert in CC3 staining at day 0 is a magnified image where the asterisk is marked. Bar graphs are quantification of Hoechst 33342 (B) and CD31 (C) densities or percentage of CC3- and CD31-double

positive vessels among all CD31-positive blood vessels (D) for subcutaneous tumors. (E) Orthotopic tumors for Hoechst 33342 perfusion dye (blue) and CD31 (red) co-immunostaining. Bar graphs are Hoechst 33342 (F) and CD31 (G) area densities. Scale bars in Figures A and E indicate 100 μm. Data in bar graphs (Figures B, C, D, F, and G) are the mean ± s.e.m. for ≥ 5 different viable regions analyzed from 2 mice per time point. *, **, and *** indicate $P<0.05$, $P<0.01$, and $P<0.005$, respectively, analyzed by 1-way analysis of variance.

however, Hoechst 33342 perfusion (Figure 9B and 9F) and CD31 density (Figure 9C and 9G) were partly restored and CC3-positive blood vessels were significantly reduced (Figure 9D), suggesting that the vessel collapse was partially restored. These data, therefore, demonstrate that the decreased F-MISO signal by PET (Figure 3B and 3C) or pimonidazole signal by FACS (Figure 7A and 7B) analyses at day 0 (i.e., 6 hours after radiation) might have resulted from insufficient intratumor perfusion of the tracers caused by the high-dose irradiation, resulting in rapid vascular collapse in the tumors.

Discussion

Although many clinical studies have demonstrated the superb efficacy and popularity of SABR, even among operable patients with stage I NSCLC, many questions remain to optimize therapy. One of the most important issues is to set an optimal fractionation schedule for SABR. At the beginning, SABR was given daily in Japan, although it is now expanded to be given at more than 72-hour intervals. With real-world circumstances such as national holidays, patient convenience, and equipment availability, the actual overall interval is 3 to 5 days (48). In the United States, the most favored schedule seemed to be approximately 54 Gy in 3 fractions within 8 to 14 days. No more than 2 fractions should be delivered each week, and a minimum of 40 hours and a maximum of 8 days are required to separate 2 fractions (26). In recent years, however, the regimen of 5 fractions of 10 Gy delivered every other day (except during the weekends) has been the most frequently used (26).

Because fractionated irradiation kills tumor cells more effectively than single treatment by the phenomenon of reoxygenation (24, 25), this process had also been extensively investigated at a single high-dose irradiation in a number of preclinical studies (30-33, 49, 50). For example, Kallman (24) has reported that reoxygenation occurs rapidly in animal tumors, starting at 100% of tumor hypoxia immediately after 15 Gy of irradiation and declining quickly by 1 hour and thereafter but never reached the pretreatment level of 1.1% in radiation-induced fibrosarcoma tumors. Similarly, Kim and Brown (31) has reported by using serial clonogenic cell survival assays that tumor hypoxia increased rapidly and returned to the pretreatment levels at 3 to 6 hours after 10 Gy of single-dose irradiation in the murine squamous cell

carcinoma VII model. Murata *et al*. (32) used paired survival curves of irradiated tumors in air breathing *versus* dead mice and showed that tumor hypoxia increased rapidly after irradiation and reoxygenation is not complete at 24 hours and proceeds further until 72 hours or thereafter after a single fraction of 13 to 15 Gy in squamous cell carcinoma VII and EMT6 murine tumors. Although these studies have all used *in vivo* clonogenic cell survival assays, the reference standard measurements of tumor response to ionizing radiation, other studies using pimonidazole immunostaining as the endpoint have demonstrated somewhat confounding results. It has been shown that a single ablative dose of irradiation (12 ~ 25 Gy) actually decreases tumor hypoxia, thereby normalizing tumor vasculature in Lewis lung carcinoma (30) and TRAMP C-1 mouse prostate cancer (33). Although these studies overall have underscored the importance of changes in tumor hypoxia after irradiation (which might be highly tumor-type dependent), all of these preclinical studies were performed in *ex vivo* subcutaneous tumor model. It is still difficult to quantify the real-time dynamic changes in tumor hypoxia with those assays.

In the present study, we used F-MISO PET imaging to investigate serial and temporal *in vivo* dynamics of tumor hypoxia in response to ablative irradiation in subcutaneous and orthotopic lung tumor models. F-MISO PET was able to detect changes in hypoxia levels after high dose of irradiation in subcutaneous lung tumors. The baseline TBR for subcutaneous lung tumors ranged from 1.71 to 4.09 indicating that considerable heterogeneity of tumor hypoxia among individual mice. Contrary to our expectations, TBR at 6 hours after irradiation was not increased compared to baseline TBR. Sudden decrease was rather observed. This pattern of hypoxic signal changes was also observed when we used a pimonidazole hypoxic probe by FACS analysis. The observed immediate decrease in F-MISO signals led us to further

examine the tumor perfusion using Hoechst 33342, a vascular perfusion dye. It is a well-established that high-dose radiation disrupts tumor vasculature (19, 45, 46). Although the previously reported studies have examined tumor vasculature at some point after irradiation (for example, 2-14 days), our results have revealed that the tumor vasculature can collapse as early as 6 hours after radiation and that the perfusion was found to be restored by the next point examined (i.e., 2 days after radiation). These results indicate that the vasculature is a very dynamic compartment within tumors, which may not completely collapse by high-dose irradiation, as suggested by some investigators (51, 52), but is reversibly recoverable, further complicating tumor reoxygenation dynamics.

On the other hands, we have used orthotopic lung tumors for this study based on the speculation that tumors grown orthotopically may be more clinically relevant model of lung tumor in which to study the biology of this disease and evaluate novel therapeutic strategies. However, elevated uptake of F-MISO above background was not evident in the current study. We hypothesize that this might have been because the orthotopic tumors were too small to yield significantly meaningful hypoxic PET imaging. It is known that the PET image does not reflect accurately the true hypoxia heterogeneity at the microregional level (53). The voxel size that would be identified in a PET imaging is much larger than most of the hypoxic regions. Thus, voxels containing low areas of hypoxia could be classified as 'negative'. Similarly to our findings, A549 lung tumors in nude mice by Graves *et al.* (54) were also reported that minimal fluoroazomycin arabinoside (F-AZA), another hypoxic PET probe, accumulation was seen in orthotopic lung tumors, whereas subcutaneous lung tumors showed substantial uptake of F-AZA. Therefore it is unlikely that the problems inherent to hypoxia PET imaging in small animals can be solved exclusively by exploiting better tracers.

Fortunately, human lung cancer is large enough to be hypoxic thus can be detected easily by hypoxia PET imaging. Indeed, several researchers have already investigated the feasibility of clinical PET imaging with various hypoxia-specific PET radiotracers, including F-MISO, F-AZA, 3-[18F]-Fluoro-2-(4-((2-nitro-1H-imidazol-1-yl)methyl)-1H-1,2,3-triazol-1-yl)propan-1-ol ([18F]-HX4), and [60Cu]-ATSM, in patients with NSCLC and assessed the potential predictive value in quantification of hypoxia (20, 22, 55-58).

There were several limitations to our study. Firstly, it would be better if we could measure the tumor hypoxia status on day 1, 3, 4, and 5. However, daily measurements were not possible due to the animals' welfare and availability of radiotracers and PET scanner. Secondly, PET scan was used in this study. CT images taken on 3 days after irradiation were used as a reference to define location of tumor and normal organs. PET/CT can give more accurate identification of the location of tumor and normal organs than PET alone. Thirdly, we used the Lewis lung carcinomas. The features of this cell which are highly tumorigenic and have metastatic potential could not properly represent the early stage lung cancer. Also, observed response to radiation in a complete murine system may not be transferable to human conditions. However, no one model can truthfully recapitulate all features of human lung cancer.

The results of the present study indicate that F-MISO PET and HRE-driven bioluminescence imaging can measure temporal changes of individual tumor hypoxia not in the orthotopic lung tumor model but in the subcutaneous lung tumor model and the heterogeneity between baseline levels of hypoxia between individual mice. After a single high-dose of irradiation, the level of tumor hypoxia returned to the pretreatment level by 2 days. Although we were not able to observe the pattern of tumor hypoxia changes in the orthotopic tumor model, our observations in the subcutaneous model might be

considered in determining the optimal fractionation schedule for SABR in the clinic. We also found that the high-dose of irradiation could induce a rapid, but reversible, vascular collapse in tumors. Future studies including patients with NSCLC treated with SABR are warranted to firmly prove the optimal fractionation schedule and predictive value of tumor hypoxia for SABR.

References

1. Torre LA, Siegel RL, Ward EM, Jemal A. Global Cancer Incidence and Mortality Rates and Trends--An Update. Cancer epidemiology, biomarkers & prevention : a publication of the American Association for Cancer Research, cosponsored by the American Society of Preventive Oncology. 2016;25(1):16-27.
2. Jung KW, Won YJ, Oh CM, Kong HJ, Cho H, Lee JK, et al. Prediction of Cancer Incidence and Mortality in Korea, 2016. Cancer research and treatment : official journal of Korean Cancer Association. 2016;48(2):451-7.
3. Humphrey LL, Deffebach M, Pappas M, Baumann C, Artis K, Mitchell JP, et al. Screening for lung cancer with low-dose computed tomography: a systematic review to update the US Preventive services task force recommendation. Annals of internal medicine. 2013;159(6):411-20.
4. Cykert S, Dilworth-Anderson P, Monroe MH, Walker P, McGuire FR, Corbie-Smith G, et al. Factors associated with decisions to undergo surgery among patients with newly diagnosed early-stage lung cancer. Jama. 2010;303(23):2368-76.
5. Loo BW, Jr., Chang JY, Dawson LA, Kavanagh BD, Koong AC, Senan S, et al. Stereotactic ablative radiotherapy: what's in a name? Practical radiation oncology. 2011;1(1):38-9.
6. Guckenberger M. Stereotactic body radiotherapy for stage I NSCLC: the challenge of evidence-based medicine. Journal of thoracic oncology : official publication of the International Association for the Study of Lung Cancer. 2014;9(2):e17-8.
7. Nagata Y. Stereotactic body radiotherapy for early stage lung cancer. Cancer research and treatment : official journal of Korean Cancer Association. 2013;45(3):155-61.
8. Zheng X, Schipper M, Kidwell K, Lin J, Reddy R, Ren Y, et al. Survival

outcome after stereotactic body radiation therapy and surgery for stage I non-small cell lung cancer: a meta-analysis. International journal of radiation oncology, biology, physics. 2014;90(3):603-11.

9. Robinson CG, DeWees TA, El Naqa IM, Creach KM, Olsen JR, Crabtree TD, et al. Patterns of failure after stereotactic body radiation therapy or lobar resection for clinical stage I non-small-cell lung cancer. Journal of thoracic oncology : official publication of the International Association for the Study of Lung Cancer. 2013;8(2):192-201.
10. Timmerman R, Paulus R, Galvin J, Michalski J, Straube W, Bradley J, et al. Stereotactic body radiation therapy for inoperable early stage lung cancer. Jama. 2010;303(11):1070-6.
11. Taremi M, Hope A, Dahele M, Pearson S, Fung S, Purdie T, et al. Stereotactic body radiotherapy for medically inoperable lung cancer: prospective, single-center study of 108 consecutive patients. International journal of radiation oncology, biology, physics. 2012;82(2):967-73.
12. Nagata Y, Takayama K, Matsuo Y, Norihisa Y, Mizowaki T, Sakamoto T, et al. Clinical outcomes of a phase I/II study of 48 Gy of stereotactic body radiotherapy in 4 fractions for primary lung cancer using a stereotactic body frame. International journal of radiation oncology, biology, physics. 2005;63(5):1427-31.
13. Baumann P, Nyman J, Hoyer M, Wennberg B, Gagliardi G, Lax I, et al. Outcome in a prospective phase II trial of medically inoperable stage I non-small-cell lung cancer patients treated with stereotactic body radiotherapy. Journal of clinical oncology : official journal of the American Society of Clinical Oncology. 2009;27(20):3290-6.
14. Le QT, Loo BW, Ho A, Cotrutz C, Koong AC, Wakelee H, et al. Results of a phase I dose-escalation study using single-fraction stereotactic radiotherapy for lung tumors. Journal of thoracic oncology : official publication of the International Association for the Study of Lung Cancer. 2006;1(8):802-9.
15. Fakiris AJ, McGarry RC, Yiannoutsos CT, Papiez L, Williams M,

Henderson MA, et al. Stereotactic body radiation therapy for early-stage non-small-cell lung carcinoma: four-year results of a prospective phase II study. International journal of radiation oncology, biology, physics. 2009;75(3):677-82.

16. Brown JM, Giaccia AJ. The unique physiology of solid tumors: opportunities (and problems) for cancer therapy. Cancer research. 1998;58(7):1408-16.
17. Moeller BJ, Richardson RA, Dewhirst MW. Hypoxia and radiotherapy: opportunities for improved outcomes in cancer treatment. Cancer metastasis reviews. 2007;26(2):241-8.
18. Brizel DM, Scully SP, Harrelson JM, Layfield LJ, Bean JM, Prosnitz LR, et al. Tumor oxygenation predicts for the likelihood of distant metastases in human soft tissue sarcoma. Cancer research. 1996;56(5):941-3.
19. Kim DW, Huamani J, Niermann KJ, Lee H, Geng L, Leavitt LL, et al. Noninvasive assessment of tumor vasculature response to radiation-mediated, vasculature-targeted therapy using quantified power Doppler sonography: implications for improvement of therapy schedules. Journal of ultrasound in medicine : official journal of the American Institute of Ultrasound in Medicine. 2006;25(12):1507-17.
20. Trinkaus ME, Blum R, Rischin D, Callahan J, Bressel M, Segard T, et al. Imaging of hypoxia with 18F-FAZA PET in patients with locally advanced non-small cell lung cancer treated with definitive chemoradiotherapy. Journal of medical imaging and radiation oncology. 2013;57(4):475-81.
21. Mandeville HC, Ng QS, Daley FM, Barber PR, Pierce G, Finch J, et al. Operable non-small cell lung cancer: correlation of volumetric helical dynamic contrast-enhanced CT parameters with immunohistochemical markers of tumor hypoxia. Radiology. 2012;264(2):581-9.
22. Dehdashti F, Mintun MA, Lewis JS, Bradley J, Govindan R, Laforest R, et al. In vivo assessment of tumor hypoxia in lung cancer with 60Cu-ATSM. European journal of nuclear medicine and molecular imaging.

2003;30(6):844-50.

23. Li L, Yu J, Xing L, Ma K, Zhu H, Guo H, et al. Serial hypoxia imaging with 99mTc-HL91 SPECT to predict radiotherapy response in nonsmall cell lung cancer. American journal of clinical oncology. 2006;29(6):628-33.
24. Kallman RF. The phenomenon of reoxygenation and its implications for fractionated radiotherapy. Radiology. 1972;105(1):135-42.
25. Kallman RF, Dorie MJ. Tumor oxygenation and reoxygenation during radiation therapy: their importance in predicting tumor response. International journal of radiation oncology, biology, physics. 1986;12(4):681-5.
26. Corso CD, Park HS, Moreno AC, Kim AW, Yu JB, Husain ZA, et al. Stage I Lung SBRT Clinical Practice Patterns. American journal of clinical oncology. 2014; PMID: 25503436.
27. Chang JY, Balter PA, Dong L, Yang Q, Liao Z, Jeter M, et al. Stereotactic body radiation therapy in centrally and superiorly located stage I or isolated recurrent non-small-cell lung cancer. International journal of radiation oncology, biology, physics. 2008;72(4):967-71.
28. Chaudhuri AA, Tang C, Binkley MS, Jin M, Wynne JF, von Eyben R, et al. Stereotactic ablative radiotherapy (SABR) for treatment of central and ultra-central lung tumors. Lung cancer. 2015;89(1):50-6.
29. Carlson DJ, Keall PJ, Loo BW, Jr., Chen ZJ, Brown JM. Hypofractionation results in reduced tumor cell kill compared to conventional fractionation for tumors with regions of hypoxia. International journal of radiation oncology, biology, physics. 2011;79(4):1188-95.
30. Lan J, Wan XL, Deng L, Xue JX, Wang LS, Meng MB, et al. Ablative hypofractionated radiotherapy normalizes tumor vasculature in lewis lung carcinoma mice model. Radiation research. 2013;179(4):458-64.
31. Kim IH, Brown JM. Reoxygenation and rehypoxiation in the SCCVII mouse tumor. International journal of radiation oncology, biology,

physics. 1994;29(3):493-7.

32. Murata R, Shibamoto Y, Sasai K, Oya N, Shibata T, Takagi T, et al. Reoxygenation after single irradiation in rodent tumors of different types and sizes. International journal of radiation oncology, biology, physics. 1996;34(4):859-65.
33. Chen FH, Chiang CS, Wang CC, Tsai CS, Jung SM, Lee CC, et al. Radiotherapy decreases vascular density and causes hypoxia with macrophage aggregation in TRAMP-C1 prostate tumors. Clinical cancer research : an official journal of the American Association for Cancer Research. 2009;15(5):1721-9.
34. Gagel B, Reinartz P, Dimartino E, Zimny M, Pinkawa M, Maneschi P, et al. pO(2) Polarography versus positron emission tomography ([(18)F] fluoromisonidazole, [(18)F]-2-fluoro-2'-deoxyglucose). An appraisal of radiotherapeutically relevant hypoxia. Strahlentherapie und Onkologie : Organ der Deutschen Rontgengesellschaft [et al]. 2004;180(10):616-22.
35. Gagel B, Piroth M, Pinkawa M, Reinartz P, Zimny M, Kaiser HJ, et al. pO polarography, contrast enhanced color duplex sonography (CDS), [18F] fluoromisonidazole and [18F] fluorodeoxyglucose positron emission tomography: validated methods for the evaluation of therapy-relevant tumor oxygenation or only bricks in the puzzle of tumor hypoxia? BMC cancer. 2007;7:113.
36. Sorensen M, Horsman MR, Cumming P, Munk OL, Keiding S. Effect of intratumoral heterogeneity in oxygenation status on FMISO PET, autoradiography, and electrode Po2 measurements in murine tumors. International journal of radiation oncology, biology, physics. 2005;62(3):854-61.
37. Tatum JL, Kelloff GJ, Gillies RJ, Arbeit JM, Brown JM, Chao KS, et al. Hypoxia: importance in tumor biology, noninvasive measurement by imaging, and value of its measurement in the management of cancer therapy. International journal of radiation biology. 2006;82(10):699-757.
38. Mason RP, Zhao D, Pacheco-Torres J, Cui W, Kodibagkar VD, Gulaka

PK, et al. Multimodality imaging of hypoxia in preclinical settings. The quarterly journal of nuclear medicine and molecular imaging : official publication of the Italian Association of Nuclear Medicine. 2010;54(3):259-80.

39. Moeller BJ, Dreher MR, Rabbani ZN, Schroeder T, Cao Y, Li CY, et al. Pleiotropic effects of HIF-1 blockade on tumor radiosensitivity. Cancer cell. 2005;8(2):99-110.
40. Kuo TH, Kubota T, Watanabe M, Furukawa T, Kase S, Tanino H, et al. Site-specific chemosensitivity of human small-cell lung carcinoma growing orthotopically compared to subcutaneously in SCID mice: the importance of orthotopic models to obtain relevant drug evaluation data. Anticancer research. 1993;13(3):627-30.
41. Liu X, Liu J, Guan Y, Li H, Huang L, Tang H, et al. Establishment of an orthotopic lung cancer model in nude mice and its evaluation by spiral CT. Journal of thoracic disease. 2012;4(2):141-5.
42. Mahy P, De Bast M, de Groot T, Cheguillaume A, Gillart J, Haustermans K, et al. Comparative pharmacokinetics, biodistribution, metabolism and hypoxia-dependent uptake of [18F]-EF3 and [18F]-MISO in rodent tumor models. Radiotherapy and oncology : journal of the European Society for Therapeutic Radiology and Oncology. 2008;89(3):353-60.
43. Liu RS, Chou TK, Chang CH, Wu CY, Chang CW, Chang TJ, et al. Biodistribution, pharmacokinetics and PET imaging of [(18)F]FMISO, [(18)F]FDG and [(18)F]FAc in a sarcoma- and inflammation-bearing mouse model. Nuclear medicine and biology. 2009;36(3):305-12.
44. Arteel GE, Thurman RG, Raleigh JA. Reductive metabolism of the hypoxia marker pimonidazole is regulated by oxygen tension independent of the pyridine nucleotide redox state. European journal of biochemistry / FEBS. 1998;253(3):743-50.
45. Park HJ, Griffin RJ, Hui S, Levitt SH, Song CW. Radiation-induced vascular damage in tumors: implications of vascular damage in ablative hypofractionated radiotherapy (SBRT and SRS). Radiation research.

2012;177(3):311-27.

46. Ahn GO, Tseng D, Liao CH, Dorie MJ, Czechowicz A, Brown JM. Inhibition of Mac-1 (CD11b/CD18) enhances tumor response to radiation by reducing myeloid cell recruitment. Proceedings of the National Academy of Sciences of the United States of America. 2010;107(18):8363-8.
47. Elmore S. Apoptosis: a review of programmed cell death. Toxicologic pathology. 2007;35(4):495-516.
48. Nagata Y, Hiraoka M, Mizowaki T, Narita Y, Matsuo Y, Norihisa Y, et al. Survey of stereotactic body radiation therapy in Japan by the Japan 3-D Conformal External Beam Radiotherapy Group. International journal of radiation oncology, biology, physics. 2009;75(2):343-7.
49. Crokart N, Jordan BF, Baudelet C, Ansiaux R, Sonveaux P, Gregoire V, et al. Early reoxygenation in tumors after irradiation: determining factors and consequences for radiotherapy regimens using daily multiple fractions. International journal of radiation oncology, biology, physics. 2005;63(3):901-10.
50. Ljungkvist AS, Bussink J, Kaanders JH, Wiedenmann NE, Vlasman R, van der Kogel AJ. Dynamics of hypoxia, proliferation and apoptosis after irradiation in a murine tumor model. Radiation research. 2006;165(3):326-36.
51. Song CW, Lee YJ, Griffin RJ, Park I, Koonce NA, Hui S, et al. Indirect Tumor Cell Death After High-Dose Hypofractionated Irradiation: Implications for Stereotactic Body Radiation Therapy and Stereotactic Radiation Surgery. International journal of radiation oncology, biology, physics. 2015;93(1):166-72.
52. Song CW, Kim MS, Cho LC, Dusenbery K, Sperduto PW. Radiobiological basis of SBRT and SRS. International journal of clinical oncology. 2014;19(4):570-8.
53. Horsman MR, Mortensen LS, Petersen JB, Busk M, Overgaard J. Imaging hypoxia to improve radiotherapy outcome. Nature reviews

Clinical oncology. 2012;9(12):674-87.

54. Graves EE, Vilalta M, Cecic IK, Erler JT, Tran PT, Felsher D, et al. Hypoxia in models of lung cancer: implications for targeted therapeutics. Clinical cancer research : an official journal of the American Association for Cancer Research. 2010;16(19):4843-52.
55. Koh WJ, Bergman KS, Rasey JS, Peterson LM, Evans ML, Graham MM, et al. Evaluation of oxygenation status during fractionated radiotherapy in human nonsmall cell lung cancers using [F-18]fluoromisonidazole positron emission tomography. International journal of radiation oncology, biology, physics. 1995;33(2):391-8.
56. Eschmann SM, Paulsen F, Reimold M, Dittmann H, Welz S, Reischl G, et al. Prognostic impact of hypoxia imaging with 18F-misonidazole PET in non-small cell lung cancer and head and neck cancer before radiotherapy. Journal of nuclear medicine : official publication, Society of Nuclear Medicine. 2005;46(2):253-60.
57. Gagel B, Reinartz P, Demirel C, Kaiser HJ, Zimny M, Piroth M, et al. [18F] fluoromisonidazole and [18F] fluorodeoxyglucose positron emission tomography in response evaluation after chemo-/radiotherapy of non-small-cell lung cancer: a feasibility study. BMC cancer. 2006;6:51.
58. Zegers CM, van Elmpt W, Reymen B, Even AJ, Troost EG, Ollers MC, et al. In vivo quantification of hypoxic and metabolic status of NSCLC tumors using [18F]HX4 and [18F]FDG-PET/CT imaging. Clinical cancer research : an official journal of the American Association for Cancer Research. 2014;20(24):6389-97.

국 문 초 록

서론: 체부정위방사선치료의 분할치료간의 적절한 시간적 간격은 확립되어 있지 않다. 종양 내 저산소화의 시간적 변화에 대한 지식은 적절한 분할치료 간격에 대한 단서를 제공할 수 있고 체부정위방사선치료의 치료 결과를 향상시킬 수 있다. 본 연구에서는 마우스 피하 폐종양 모델과 정위 폐종양 모델에서 일회 고선량 방사선 조사 후 연속적인 생체 내 종양의 저산소화 측정이 F-MISO PET영상법과 HRE유도생체발광영상법에 의해 가능할 것으로 가설을 세웠다. 또한 마우스 폐종양 모델에서 종양 내 저산소화가 방사선 조사 후 6시간 내지 6일 째에 치료 전 수준으로 돌아올 것으로 가설을 세웠다.

방법: 동계 루이스 폐종양을 C57BL/6 마우스의 등쪽 피하와 폐에 자라게 한 이후, 임상에서 사용되는 체부정위방사선치료와 유사한 효과를 내기 위해 일 회 선량, 15 Gy를 조사하였다. 피하폐종양과 정위폐종양 모두에서 방사선 조사 전(day -1), 조사 6시간 후(day 0), 조사 2일 후(day 2), 그리고 조사 6일 후(day 6)에 연속적인 F-MISO PET영상을 획득하였다. 종양의 배경에 대한 F-MISO의 활성도 비(TBR)를 분석하였다. HRE유도생체발광영상은 방사선 조사 6시간 후, 조사 1일 후, 2일 후, 6일 후에 시행하였다. F-MISO PET영상과 생체발광영상의 실험결과를 더 잘 설명하기 위해 Pimonidazole FACS분석과 면역염색을 함께 한 Hoechst 33342 혈관내 관류 분석 또한 시행하였다.

결과: 피하종양에서 최대 TBR은 day -1에 2.87 ± 0.483, day 0에

1.67 ± 0.116, day2에 2.92 ± 0.334, 그리고 day 6에 2.13 ± 0.385였고, 이는 종양 내 저산소화가 방사선 조사 후 급격히 감소한 후, 조사 후 2일째에서 조사 전 수준으로 돌아온 것을 뜻하였다. 정위 폐종양모델은 F-MISO PET영상법과 HRE유도생체발광영상 모두에서 저산소화 신호가 너무 약하여 정량화할 수 없었다. Pimonidazole FACS분석 역시 유사한 패턴을 보였다. 즉, pimonidazole이 양성인 세포 수가 방사선 조사 후 급격히 감소한 후 조사 전의 수준으로 회복되었다. Hoechst 33342 혈관내 관류 인자와, CD31과 cleaved caspase 3의 공동 면역염색을 이용하여, 급속하지만 일시적인 혈관 허탈이 있었음을 발견하였다. 이로 인해 방사선 조사 후 6시간 째에 F-MISO PET 표지자와 pimonidazole의 종양 내 불량한 관류를 일으켰을 수 있다. 그리하여 PET과 pimonidazole분석에서 방사선 조사 후 6시간 째에, 저산소화 신호가 감소되어 나타난 원인일 수도 있다.

결론: F-MISO PET영상법과 HRE유도생체발광영상법은 마우스 피하 폐종양 모델에서는 개별 종양의 저산소화의 시간적 변화를 정량화 할 수 있었지만, 정위폐종양 모델에서는 정량화하지 못하였다. 마우스 피하 폐종양 모델에서, 일 회 고선량 방사선 조사 후, 종양 내 저산소화의 수준은 조사 후 2일 내에 조사 전 수준으로 돌아왔다. 또한 본 연구는, 일 회 고선량 방사선 조사가 종양 내 혈관의 가역적이나 급속한 허탈을 발생시킬 수 있음을 보여주었다.

* 본 내용은 미국방사선종양학회지 (International journal of radiation oncology, biology, physics. 2016;95(3):1022-31)에 출판 완료된 내용임.

주요어: 폐암, 저산소증, 양전자방출단층촬영, 방사선치료, 선량분할

학 번: 2013-30548